A. Zaib*, A. J. Chamkha, M. M. Rashidi, and K. Bhattacharyya

Impact of nanoparticles on flow of a special non-Newtonian third-grade fluid over a porous heated shrinking sheet with nonlinear radiation

https://doi.org/10.1515/nleng-2017-0033
Received March 2, 2017; accepted October 1, 2017.

Abstract: This research peruses the characteristics of heat and mass transfer of a special non-Newtonian third-grade fluid over a porous convectively-heated shrinking sheet filled with nanoparticles. The Buongiorno model is used for the special non-Newtonian third-grade fluid that includes both the Brownian motion and the thermophoresis effects with non-linear radiation. The nonlinear system of ordinary differential equations are obtained using a suitable transformation. The converted system of equations are then numerically solved using shooting method. The numerically-obtained results for the skin friction, local Nusselt number and the local Sherwood number as well as velocity profile, temperature distribution and concentration of nanoparticle are illustrated for different physical parameters through graphs and tables. On the behalf of the whole studies, final conclusions are made and it is observed that multiple solutions are achieved for certain values of the suction parameter. Further, the non-Newtonian parameter reduces the velocity of the fluid and increases the temperature and the concentration profiles for the first solution while the reverse trend is seen for the second solution. Finally, a comparative analysis is made through previous studies in limiting cases and shown good correlation.

Keywords: Nanofluid; special third-grade fluid; nonlinear radiation; Buongiorno model; convective boundary condition

PACS: 44.20.+b; 44.40.+a; 47. 50.-d

1 Introduction

The intention in boundary layer flow of a non-Newtonian fluid is raising significantly due to numerous practical applications in manufacturing and industrial processes. Molten plastics, blood, ketchup, greases, artificial fibers, paint, certain oils and many more are examples of non-Newtonian fluid. These fluids disobey the well-known law of Newton's viscosity and as these fluids are highly viscous which do reveal their significant properties of elastic. These types of fluids arise in a broad variety of realistic problems having imperative importance in composite processing, polymer depolarization, bubble absorption and boiling, etc. Therefore, the study of the behavior of non-Newtonian fluid of such types is essential. At present, the non-Newtonian fluids are examined through three major categories such as the rate type, differential type and the integral type. The second-grade fluid is known as a subclass fluid of the differential type model which exhibits the effect of the normal stress and cannot predict the shear thinning and shear thickening phenomena. On the other hand, the model of the third-grade fluid can predict both the normal stresses as well as the shear thinning and the shear thickening phenomena even the constitutive equations have many complexities. Several researchers have investigated the flows of this model under many different aspects [1–5]. Recently, Naganthran et al. [6] obtained the dual solutions of a special third-grade fluid towards a stagnation-point of an unsteady porous stretching/ shrinking surface. They found that the multiple solutions exist for a stretching sheet as well as for a shrinking sheet. Also, they showed that the first solution is stable and realizable physically by the stability analysis while the second solution is unstable.

The phenomenon of enhancement of the thermal conductivity of fluid by scattering nanoparticles was scrutinized by Masuda et al. [7]. Buongiorno [8] observed

***Corresponding Author: A. Zaib,** Department of Mathematical Sciences, Federal Urdu University of Arts, Science & Technology, Gulshan-e-Iqbal Karachi-75300, Pakistan, E-mail: zaib20042002@yahoo.com
A. J. Chamkha, Mechanical Engineering Department, Prince Mohammad Bin Fahd University, Al-Khobar 31952, Saudi Arabia
M. M. Rashidi, Department of Civil Engineering, School of Engineering, University of Birmingham, Birmingham, UK
K. Bhattacharyya, Department of Mathematics, Institute of Science, Banaras Hindu University, Varanasi-221005, Uttar Pradesh, India

that the Brownian motion and thermophoresis effects of nanoparticles give the fabulous enhancement in fluid's thermal conductivity. Due to these effects, he suggested the modifications in the convective situations. Khan and Pop [9] obtained the numerical solution of nanofluid past a stretching sheet using Buongiorno's model and analyzed the Brownian motion and the thermophoresis effects on the heat transfer rate at the surface. Further, this problem was extended by Rana and Bhargava [10] by considering a nonlinear stretching surface. The characteristics of heat transfer in nanofluid over a stretching sheet in the presence of convective boundary condition was examined by Makinde and Aziz [11]. They observed that the thermal characteristics can be considerably changed by increasing the effects of Brownian motion and thermophoresis. Chamkha and co-workers have investigated various aspects of heat and mass transfer on a nanofluid flow over plates and stretching sheets under various conditions [12–15]. Recently, Krishnamurthy et al. [16] scrutinized the combined effects of thermal radiation and melting heat transfer on flow of nanofluid towards a nonlinear stretching sheet with slip effect and chemical reaction.

The thermal radiation effect with a convective boundary condition is engaged in many engineering and industrial processes containing die forging, gas turbines, chemical reactions, nuclear turbines and storage of thermal energy. Aziz [17] examined the boundary layer flow past a flat plate with convective boundary conditions. Makinde and Aziz [18] investigated MHD mixed convection boundary layer flow and heat transfer over a heated vertical plate immersed in porous medium. The boundary layer flow with heat transfer towards a heated porous stretching surface was investigated numerically by Ishak [19]. Yao et al. [20] found an exact solution for boundary layer flow past a convectively heated permeable stretching/shrinking wall. Rahman et al. [21] studied mixed convective flow past a vertical flat plate in the presence of convective boundary condition. Mustafa et al. [22] investigated the Maxwell fluid over a heated exponentially stretching surface immersed in a nanofluid. Ibrahim and Haq [23] studied the MHD flow of a nanofluid towards a stagnation-point past a stretching surface with convective boundary condition. Makinde et al. [24] illustrated MHD stagnation-point flow of a nanofluid past a connective heated stretching sheet with slip and radiation effects. Recently, Khan et al. [25] studied the effect of nonlinear radiation on MHD flow of a Carreau fluid past a nonlinear stretching surface through convective boundary condition.

The aim of this study is to consider the boundary-layer flow of a special non-Newtonian third-grade fluid past a convectively heated shrinking sheet with the nonlinear thermal radiation due to solar energy. The Buongiorno model is used for the third-grade fluid which includes both the Brownian motion and the thermophoresis effects. The transformed nonlinear equations are solved numerically using shooting method. As far our knowledge, the objective which has been considered in this research is still to be ruminated over and therefore yet no to be communicated.

2 Mathematical Formulation

Consider a steady two dimensional laminar flow with heat and mass transfer of a special non-Newtonian fluid past a heated shrinking sheet with nonlinear thermal radiation filled with nanoparticles. It is presumed that x-axis measured along the shrinking sheet and y-axis normal to it. It is also assumed that the shrinking surface velocity is $u_w(x) = ax$ with $a > 0$. Further, it is assumed that at the lower surface, the sheet is heated convectively with a temperature T_f which provides a heat transfer coefficient h_f. The physical equations that govern the steady flow are written as (Naganthran et al. [6] and Mustafa et al. [22]):

$$\frac{\partial u}{\partial x} + \frac{\partial v}{\partial y} = 0 \tag{1}$$

$$u\frac{\partial u}{\partial x} + v\frac{\partial u}{\partial y} = \nu\frac{\partial^2 u}{\partial y^2} + 6\kappa\left(\frac{\partial u}{\partial y}\right)^2\frac{\partial^2 u}{\partial y^2} \tag{2}$$

$$u\frac{\partial T}{\partial x} + v\frac{\partial T}{\partial y} = \alpha\frac{\partial^2 T}{\partial y^2} + \Lambda\left[D_B\frac{\partial C}{\partial y}\frac{\partial T}{\partial y} + \left(\frac{D_T}{T_\infty}\right)\left(\frac{\partial T}{\partial y}\right)^2\right] - \frac{1}{(\rho c_p)_f}\frac{\partial q_r}{\partial y} \tag{3}$$

$$u\frac{\partial C}{\partial x} + v\frac{\partial C}{\partial y} = D_B\frac{\partial^2 C}{\partial y^2} + \left(\frac{D_T}{T_\infty}\right)\left(\frac{\partial T^2}{\partial y^2}\right) \tag{4}$$

The physical boundary conditions are

$$u = -u_w(x), v = -v_0, -k\frac{\partial T}{\partial y} = h_f\left(T_f - T\right), C = C_w \text{ at } y = 0,$$
$$u \to 0, T \to T_\infty, C \to C_\infty \text{as} y \to \infty. \tag{5}$$

where u and v are the velocity components in the x– and y–axes, respectively, α is the thermal diffusivity, ν is the kinematic viscosity, ρ is the density, T is the temperature, T_∞ is the free stream temperature, T_f is the convective fluid temperature, C is the concentration of nanoparticle, D_B and D_T are the coefficients of Brownian and thermophoresis diffusion, respectively, κ is the non-Newtonian parameter, Λ is the ratio between the effective heat capacity of the

nanoparticle material and specific heat capacitance of the fluid, $(\rho c_p)_f$ is the specific heat capacitance of nanofluid.

Following Khan et al. [25], the radiative heat flux q_r is expressed as

$$q_r = -\frac{4\sigma^*}{3k^*}\frac{\partial T}{\partial y} = -\frac{16\sigma^*}{3k^*}T^3\frac{\partial T}{\partial y} \tag{6}$$

where σ^* is the Stefan–Boltzmann constant and is the mean absorption coefficient. Using Eq. (6), Energy Eq. (3) can be written as

$$u\frac{\partial T}{\partial x} + v\frac{\partial T}{\partial y} = \frac{\partial}{\partial y}\left[\left(\alpha + \frac{16\sigma^* T^3}{3(\rho c_p)_f k^*}\right)\frac{\partial T}{\partial y}\right] + \Lambda\left[D_B\frac{\partial C}{\partial y}\frac{\partial T}{\partial y} + \left(\frac{D_T}{T_\infty}\right)\left(\frac{\partial T}{\partial y}\right)^2\right] \tag{7}$$

Now, we introduce the similarity transformation:

$$\eta = y\sqrt{\frac{a}{\nu}},\ \psi = \sqrt{a\nu}xf(\eta),$$
$$\theta(\eta) = \frac{T - T_\infty}{T_f - T_\infty},\ \phi(\eta) = \frac{C - C_\infty}{C_w - C_\infty}. \tag{8}$$

Here η is the similarity variable,ψ is the stream function and we get $T = T_\infty[1 + (\theta_w - 1)\theta]$ with $\theta_w > 1$, where $\theta_w = \frac{T_f}{T_\infty}$ is being the temperature ratio parameter. Here for similarity solution, we assumed that $\kappa = \kappa_0/x^2$, where $\kappa_0 > 0$ being a constant (see Naganthran et al. [6] and Ishak [19]).

In view of relation (8), Eqs. (2), (4) and (7) are transmuted into the following equations:

$$(1 + Kf''^2)f''' + ff'' + f'^2 = 0 \tag{9}$$

$$\theta'' + \Pr f\theta' + \frac{4}{3R_d}\frac{d}{d\eta}\left[\{1 + (\theta_w - 1)\theta\}^3\theta'\right] + \Pr\left[Nb\theta'\phi' + Nt(\theta')^2\right] = 0 \tag{10}$$

$$\phi'' + Lef\phi' + \frac{Nt}{Nb}\theta'' = 0 \tag{11}$$

subject to the following boundary conditions:

$$f(0) = S,\ f'(0) = -1,\ \theta'(0) = -\gamma\left(1 - \theta(0)\right),\ \phi(0) = 1,\ f'(\infty) \to 0,\ \theta(\infty) \to 0, \phi(\infty) \to 0. \tag{12}$$

where the prime denotes differentiation with respect to η, $K = 6\kappa_0 a^3/\nu^2$ is the dimensionless non-Newtonian parameter, $\Pr = \nu/\alpha$ is the Prandtl number, $Nb = \tau D_B(C_w - C_\infty)/\nu$ is the Brownian motion parameter, $Nt = \tau D_T\left(T_f - T_\infty\right)/T_\infty\nu$ is the thermophoresis parameter, $\gamma = h_f\sqrt{\nu/a}/k$ is the convective parameter, $R_d = kk^*/4\sigma^* T_\infty^3$ is the thermal radiation parameter, $S = v_0/\sqrt{a\nu} > 0$ is the suction parameter and $Le = \nu/D_B$ is the Lewis parameter.

The important physical quantities of interest are the local skin-friction coefficient, the local Nusselt number and the local Sherwood number are defined as:

$$C_{fx} = \frac{\tau_w}{\rho u_w^2},\ Nu_x = -\frac{xq_w}{k(T_f - T_w)},\ Sh_x = \frac{xm_w}{D_B(C_w - C_\infty)}, \tag{13}$$

where τ_w is the shear stress in x–direction (see Naganthran et al. [6]), q_w is the heat flux and m_w is the mass flux given as

$$\tau_w = \mu\left(\frac{\partial u}{\partial y}\right)_{y=0}, q_w = -k\left(\frac{\partial T}{\partial y}\right)_w + (q_r)_w, m_w = -D_B\left(\frac{\partial C}{\partial y}\right)_{y=0}, \tag{14}$$

Using (8), we get

$$C_f\mathrm{Re}_x^{1/2} = f''(0),\ Sh_x\mathrm{Re}_x^{-1/2} = -\phi'(0),$$
$$Nu_x\mathrm{Re}_x^{-1/2} = -\left[1 + \tfrac{4}{3R_d}\left\{1 + (\theta_w - 1)\theta(0)\right\}^3\right]\theta'(0). \tag{15}$$

where $Re_x = xu_w(x)/\nu$ is the Reynolds number.

3 Stability Analysis

As suggested by Merkin [27] and Weidman et al. [28], we test the stability analysis by taking the unsteady form of Eqs. 1–4.

$$\frac{\partial u}{\partial x} + \frac{\partial v}{\partial y} = 0 \tag{16}$$

$$\frac{\partial u}{\partial t} + u\frac{\partial u}{\partial x} + v\frac{\partial u}{\partial y} = \nu\frac{\partial^2 u}{\partial y^2} + 6\kappa\left(\frac{\partial u}{\partial y}\right)^2\frac{\partial^2 u}{\partial y^2} \tag{17}$$

$$\frac{\partial T}{\partial t} + u\frac{\partial T}{\partial x} + v\frac{\partial T}{\partial y} = \alpha\frac{\partial^2 T}{\partial y^2} + \tau\left[D_B\frac{\partial C}{\partial y}\frac{\partial T}{\partial y} + \left(\frac{D_T}{T_\infty}\right)\left(\frac{\partial T}{\partial y}\right)^2\right] - \frac{1}{(\rho c_p)_f}\frac{\partial q_r}{\partial y} \tag{18}$$

$$\frac{\partial C}{\partial t} + u\frac{\partial C}{\partial x} + v\frac{\partial C}{\partial y} = D_B\frac{\partial^2 C}{\partial y^2} + \left(\frac{D_T}{T_\infty}\right)\left(\frac{\partial^2 T}{\partial y^2}\right) \tag{19}$$

where t represents the time. This introduce a new variable in similarity transformation:

$$\eta = y\sqrt{\frac{a}{\nu}}, \psi = \sqrt{a\nu}xf(\eta,\tau), \theta(\eta,\tau) = \frac{T - T_\infty}{T_f - T_\infty},$$
$$\phi(\eta,\tau) = \frac{C - C_\infty}{C_w - C_\infty}, \tau = at. \tag{20}$$

Using Eq. (20), Eqs. (17)–(19) can be written as

$$\left(1 + K\left(\frac{\partial^2 f}{\partial\eta^2}\right)^2\right)\frac{\partial^3 f}{\partial\eta^3} + f\frac{\partial^2 f}{\partial\eta^2} - \left(\frac{\partial f}{\partial\eta}\right) - \frac{\partial^2 f}{\partial\eta\partial\tau} = 0 \tag{21}$$

$$\left[3R_d + 4\left(1 + (\theta_w - 1)\theta\right)^3\right]\frac{\partial^2\theta}{\partial\eta^2} + 3\,\mathrm{Pr}\,R_d f\frac{\partial\theta}{\partial\eta} + 12(\theta_w - 1)\left(1 + (\theta_w - 1)\theta\right)^2\left(\frac{\partial\theta}{\partial\eta}\right)^2 + 3R_d\,\mathrm{Pr}\left(Nb\frac{\partial\theta}{\partial\eta}\frac{\partial\phi}{\partial\eta} + Nt\left(\frac{\partial\theta}{\partial\eta}\right)^2\right) - 3\,\mathrm{Pr}\,R_d\frac{\partial\theta}{\partial\tau} = 0 \tag{22}$$

$$\frac{\partial^2\phi}{\partial\eta^2} + Lef\frac{\partial\phi}{\partial\eta} + \frac{Nt}{Nb}\frac{\partial^2\theta}{\partial\eta^2} - Le\frac{\partial\phi}{\partial\tau} = 0 \tag{23}$$

subject to the following boundary conditions

$$f(0,\tau) = S,\ \frac{\partial f}{\partial\eta}(0,\tau) = -1,\ \frac{\partial\theta}{\partial\eta}(0,\tau) = -\gamma[1 - \theta(0,\tau)],$$
$$\phi(0,\tau) = 1,\ \frac{\partial f(\eta,\tau)}{\partial\eta} \to 0,\ \theta(\eta,\tau) \to 0,\ \phi(\eta,\tau) \to 0 \quad \text{as} \quad \eta \to \infty. \tag{24}$$

To test the stability of the steady flow solution $f(\eta) = f_0(\eta), \theta(\eta) = \theta_0(\eta)$, and $\phi(\eta) = \phi_0(\eta)$ satisfying the boundary value problem (9)–(11), we can write

$$\begin{aligned} f(\eta,\tau) &= f_0(\eta) + e^{-\alpha\tau}F(\eta,\tau),\\ \theta(\eta,\tau) &= \theta_0(\eta) + e^{-\alpha\tau}G(\eta,\tau),\\ \phi(\eta,\tau) &= \phi_0(\eta) + e^{-\alpha\tau}H(\eta,\tau), \end{aligned} \tag{25}$$

where α is an unknown eigenvalue, $F(\eta,\tau)$, $G(\eta,\tau)$ and $H(\eta,\tau)$ are small relative to $f_0(\eta)$, $\theta_0(\eta)$ and $\phi_0(\eta)$. Substituting (25) into (21)–(23), we get the following linearized equations

$$(1 + Kf_0''^2)\frac{\partial^3 F}{\partial\eta^3} + (f_0 + 2Kf_0'' + f_0''')\frac{\partial^2 F}{\partial\eta^2} - 2f_0'\frac{\partial F}{\partial\eta} + f_0''F - \frac{\partial^2 F}{\partial\eta\partial\tau} + \alpha\frac{\partial F}{\partial\eta} = 0 \tag{26}$$

$$(3R_d + 4)\frac{\partial^2 G}{\partial\eta^2} + 3PrR_d\left(f_0\frac{\partial G}{\partial\eta} + \theta_0'F\right) + 3R_dPrNb\left(\theta_0'\frac{\partial H}{\partial\eta} + \phi_0'\frac{\partial G}{\partial\eta}\right) + 6R_dPrNt\theta_0'\frac{\partial G}{\partial\eta} + 4(\theta_w - 1)\begin{bmatrix} +6\theta_0'\frac{\partial G}{\partial\eta} + 3(\theta_w - 1)\left(\theta_0\frac{\partial^2 G}{\partial\eta^2} + \theta_0''G\right)\\ +6(\theta_w - 1)\left(2\theta_0\theta_0'\frac{\partial G}{\partial\eta} + \theta_0'^2 + G\right)\\ +(\theta_w - 1)^2\left(\theta_0^3\frac{\partial^2 G}{\partial\eta^2} + \theta_0^2\theta_0''G\right)\\ +3(\theta_w - 1)^2\left(\theta_0^2\frac{\partial^2 G}{\partial\eta^2} + 2\theta_0\theta_0''G\right)\\ +6(\theta_w - 1)^2\left(\theta_0^2\theta_0'\frac{\partial G}{\partial\eta} + \theta_0\theta_0'^2G\right)\end{bmatrix} + 3PrR_d\alpha G - 3PrR_d\frac{\partial G}{\partial\tau} = 0 \tag{27}$$

$$\frac{\partial^2 H}{\partial\eta^2} + Le\left(f_0\frac{\partial H}{\partial\eta} + \phi_0' + F\right) + \frac{Nt}{Nb}\frac{\partial^2 G}{\partial\eta^2} + Le\left(\alpha H - \frac{\partial H}{\partial\tau}\right) = 0 \tag{28}$$

along with the boundary conditions

$$F(0,\tau) = 0,\ \frac{\partial F}{\partial\eta}(0,\tau) = 0,\ \frac{\partial G}{\partial\eta}(0,\tau) = \gamma G(0,\tau),$$
$$H(0,\tau) = 0,\ \frac{\partial F(\eta,\tau)}{\partial\eta} \to 0,\ G(\eta,\tau) \to 0,\ H(\eta,\tau) \to 0 \quad \text{as} \quad \eta \to \infty. \tag{29}$$

As proposed by Weidman et al. [28], we analyze the stability of the steady flow and heat transfer solution $f_0(\eta)$, $\theta_0(\eta)$ and $\phi_0(\eta)$ by setting $\tau = 0$, and thus $F = F_0(\eta)$, $G = G_0(\eta)$ and $H = H_0(\eta)$ in (26)–(29) to identify initial growth or decay of the solution (25). To test our numerical procedure we have to solve the linear eigenvalue problem

$$(1 + Kf_0''^2)F_0'''' + (f_0 + 2Kf_0''f_0'''')F_0'' - 2f_0'F_0' + f_0''F_0 + \alpha F_0' = 0 \tag{30}$$

$$(3R_d + 4)G_0'' + 3PrR_d(f_0G_0' + \theta_0'F_0) + 3R_dPrNb(\theta_0'H_0' + \phi_0'G_0') + 6R_dPrNt\theta_0'G_0' + 4(\theta_w - 1)\begin{bmatrix} 6\theta_0'G_0' + 3(\theta_w - 1)(\theta_0G_0'' + \theta_0''G_0)\\ +6(\theta_w - 1)(2\theta_0\theta_0'G_0' + \theta_0'^2G_0)\\ +(\theta_w - 1)^2(\theta_0^3G_0'' + \theta_0^2\theta_0''G_0)\\ +3(\theta_w - 1)^2(\theta_0^2G_0'' + 2\theta_0\theta_0''G_0)\\ +6(\theta_w - 1)^2(\theta_0^2\theta_0'G_0' + \theta_0\theta_0'^2G_0)\end{bmatrix} + 3PrR_d\alpha G_0 = 0 \tag{31}$$

$$H_0'' + Le(f_0H_0' + \phi_0'F_0) + \frac{Nt}{Nb}G_0'' + Le\alpha H_0 = 0 \tag{32}$$

along with the boundary conditions

$$F_0(0) = 0,\ F_0'(0) = 0,\ G_0'(0) = \gamma G_0(0),$$
$$H_0(0) = 0,\ F_0'(\eta) \to 0,\ G_0(\eta) \to 0,\ H_0(\eta) \to 0 \ \text{ as } \ \eta \to \infty. \tag{33}$$

It is worth mentioning that for a particular values of physical parameters, the corresponding steady flow solution $f_0(\eta)$, $\theta_0(\eta)$ and $\phi_0(\eta)$, the stability of the steady flow solution is determined by the smallest eigenvalue α. Solutions of the problem (30)–(32) give an infinite set of eigenvalues $\alpha_1 < \alpha_2 < \alpha_3 < \ldots$; if the smallest eigenvalue is positive ($\alpha_1 \geq 0$) then there is an initial decay of disturbances and the flow is stable, and if is negative then there is an initial growth of disturbances, which indicates that the flow is unstable. As suggested by Harris et al. [29], the range of possible eigenvalues can be obtained by relaxing a boundary condition on $F_0(\eta)$ or $G_(\eta)$ or $H_0(\eta)$. For the current problem, we relax the condition $G_0(\eta) \to 0$ as and for a fixed value of , we solve the system of equations (30)–(32) subject to the boundary conditions (33), along with the new boundary condition $G_0'(0) = 1$.

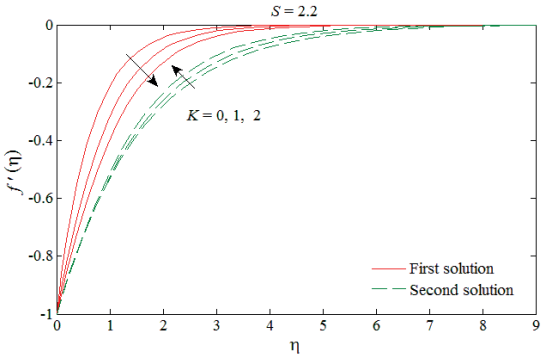

Fig. 1: The velocity profiles for different values of K.

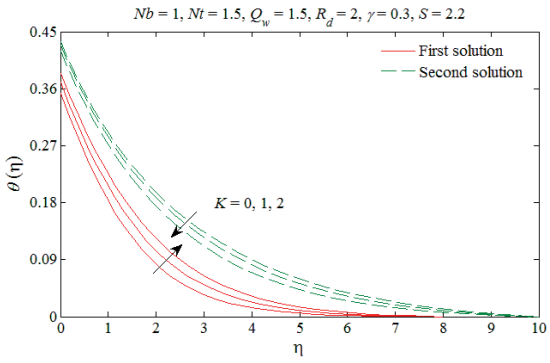

Fig. 2: The temperature profiles for different values of K.

4 Results and discussion

The set of transmuted non-linear equations (9)–(11) along with the boundary condition (12) are numerically solved using shooting method. The obtained numerical results for different physical parameters involving in the problem are discussed through graphs and tables. Table 1 displays the comparison of our results of $-\theta'(0)$ and $-\phi'(0)$ with the available results in a limiting cases and show good agreement.

The velocity, temperature distribution and the concentration of nanoparticle for different values of the non-Newtonian parameter K are depicted in Figs. 1–3. Fig. 1 shows that the velocity profile decreases with increasing values of K for the first solution and therefore, the momentum boundary layer thickness increases while for the second solution, the velocity profile increases. On the other hand, the temperature distribution and concentration of nanoparticle increase with K for the first solution as portrayed in Figs. 2 and 3 and consequently, the thermal and concentration boundary layers increase. It is also found from these figures that the velocity, temperature and the concentration of nanoparticle are larger for the special third-grade fluid compared with the Newtonian fluid (K = 0). Further, these profiles satisfy the boundary conditions asymptotically and the existence of multiple solutions that support the validation of our obtained numerical results.

Fig. 4 shows that due to increasing the value of the Brownian parameter Nb, the temperature profile increases, whereas the opposite behavior is observed for the concentration profile as shown in Fig. 5. Thus, the thermal boundary layer thickness increases, whereas the concentration boundary layer thickness decreases. This is due to the fact that the kinetic energy of the nanoparticles increases due to the strength of this chaotic motion and as a result, the fluids temperature increases. This is because the Brownian motion at the nanoscale and the molecu-

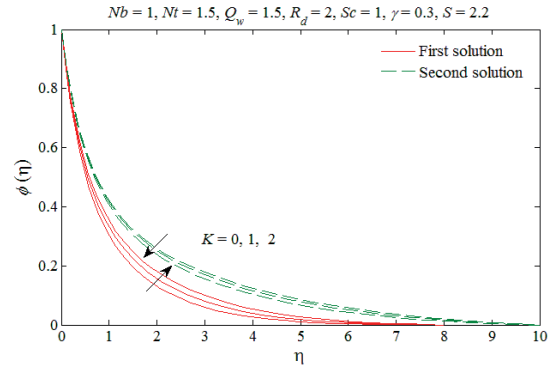

Fig. 3: The concentration profiles for different values of K.

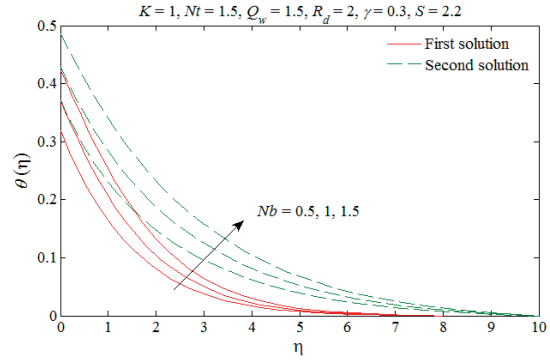

Fig. 4: The temperature profiles for different values of Nb.

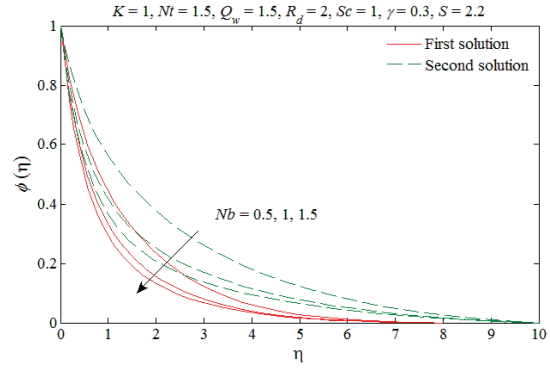

Fig. 5: The concentration profiles for different values of Nb.

Table 1: Comparison of $-\theta'(0)$ and $-\phi'(0)$ when $S = 0$, $\Pr = Le = 10$, $R_d = \gamma = \infty$ in case of stretching sheet $f'(0) = 1$.

Nt	Nb	Makinde and Aziz [27]		Present	
		$-\theta'(0)$	$-\phi'(0)$	$-\theta'(0)$	$-\phi'(0)$
0.1	0.1	0.9524	2.1294	0.9524	2.1294
0.2	0.1	0.5056	2.3819	0.5056	2.3819
0.3	0.1	0.2522	2.4100	0.2522	2.4100
0.4	0.1	0.1194	2.3997	0.1194	2.3997
0.5	0.1	0.0543	2.3836	0.0543	2.3836
0.1	0.2	0.6932	2.2740	0.6932	2.2740
0.1	0.3	0.5201	2.5286	0.5201	2.5286
0.1	0.4	0.4026	2.7952	0.4026	2.7952
0.1	0.5	0.3211	3.0351	0.3211	3.0351

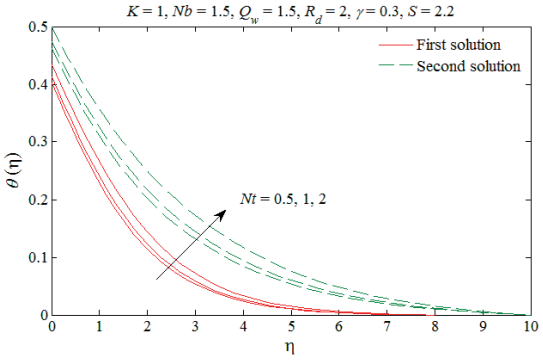

Fig. 6: The temperature profiles for different values of Nt.

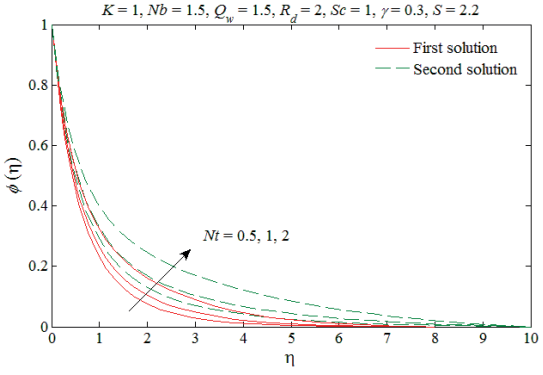

Fig. 7: The concentration profiles for different values of Nt.

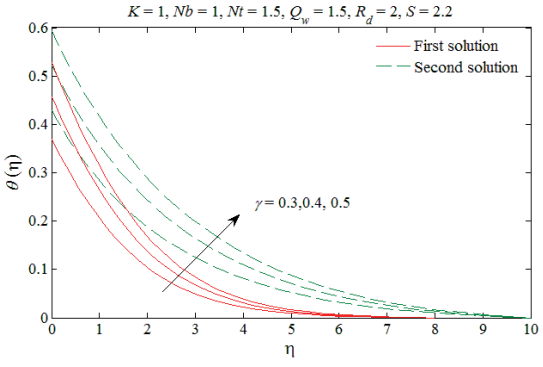

Fig. 8: The temperature profiles for different values of γ.

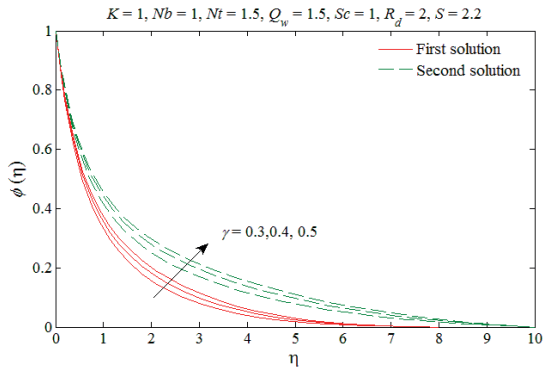

Fig. 9: The concentration profiles for different values of γ.

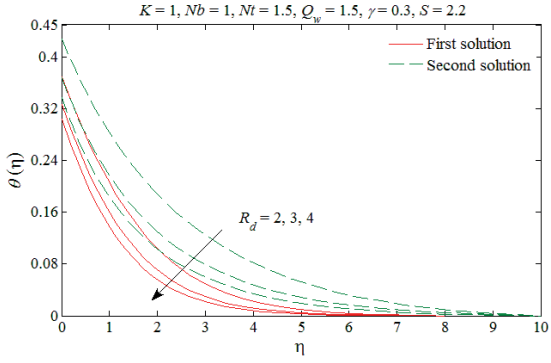

Fig. 10: The temperature profiles for different values of R_d.

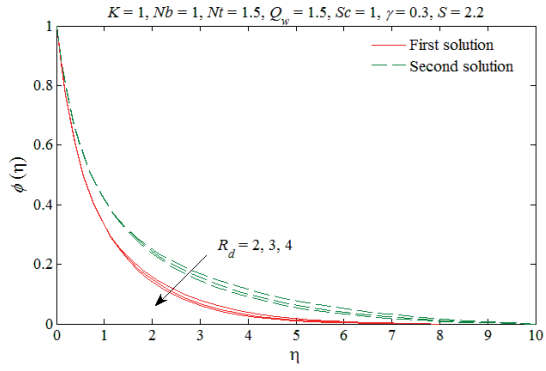

Fig. 11: The concentration profiles for different values of R_d.

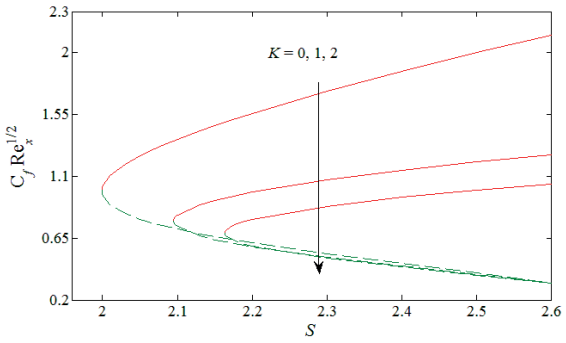

Fig. 12: The skin friction $C_f \mathrm{Re}_x^{1/2}$ versus S for different values of K.

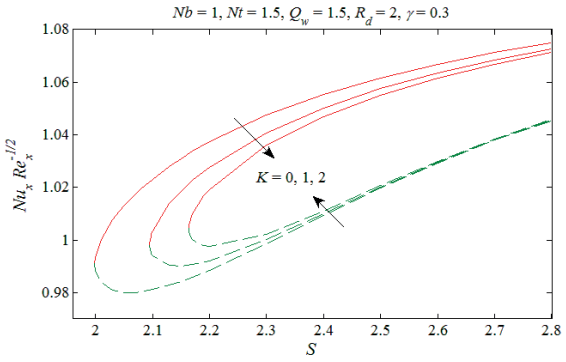

Fig. 13: The Nusselt number $Nu_x \mathrm{Re}_x^{-1/2}$ versus S for different values of K.

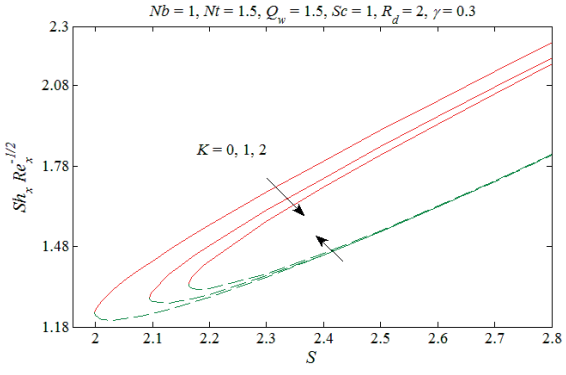

Fig. 14: The Sherwood number $Sh_x \mathrm{Re}_x^{-1/2}$ versus S for different values of K.

lar levels is an important mechanism of the nanoscale level that governs the thermal behaviors. In systems using nanofluids, the Brownian motion takes place because of the size of nanoparticles which can change the properties of heat transfer. As the scale size of particles approaches the scale of nanometer, the particles Brownian motion and its result on the surrounding liquids play a vital role in heat transfer characteristics. Figs. 6 and 7 show the effects of the thermophoresis parameter Nt on the temperature and the concentration of nanoparticle. These figures show that the temperature profile and the concentration of nanoparticle increase with increasing Nt. This is because diffusion penetrates deeper into the fluid due to increasing values of Nt which causes the thickening of the thermal boundary layer as well as the concentration boundary layer.

The effect of the convective parameter γ on the temperature distribution and concentration of nanoparticle are perused in Figs. 8 and 9, respectively. Fig. 8 reveals that due to the increase in the value of γ resulting from the stronger convective heating at the surface, the temperature gradient at the surface of the sheet increases. This allows the thermal effect to penetrate deeper into the quiescent fluid. Therefore, the temperature and the thermal boundary layer thickness increase with increasing values of γ for the first and second solutions. It is worth mentioning that the constant wall temperature $\theta(0) = 1$ can be recovered by taking sufficiently large values of the convective parameter. Further $\gamma = 0$ corresponds to the case of an insulated sheet. Fig. 9 shows that the concentration of nanoparticle as well as the concentration boundary layer increases with larger values of γ for both solutions. Figs. 10 and 11 show that the temperature and the concentration of nanoparticle decrease as the radiation parameter R_d increases for the first solution as well as for the second solution. Thus, the thermal and concentration boundary layers thicknesses become thinner and thinner for both solutions. This is due to the fact that a large value of the radiation parameter implies the dominance of conduction and therefore, the thermal and concentration boundary layer thicknesses decrease.

The skin-friction coefficient $C_f Re_x^{1/2}$, the Nusselt number $Nu_x Re_x^{-1/2}$ and the Sherwood number $Sh_x \mathrm{Re}_x^{-1/2}$ versus S for different values of the non-Newtonian parameter [$K = 0$ (Newtonian fluid), 1,2] are illustrated in Figs. 12–14, respectively and in Table 2. Fig. 12 shows that the skin friction decreases with increasing K for first solution as well as for second solution. On the other hand, the values of the Nusselt number and the Sherwood number also decrease with increasing K in case of the first solution, while the values increase for the second solution as shown in Figs. 13 and 14. The behavior of these results is also shown through Table 2. Dual solutions are achieved for $S \geq S_c$ and no solution for $S < S_c$ where S_c is the critical value of S. Further, the critical values has been displayed in Table 3. The larger characteristics of the non-Newtonian special third-grade fluid increase the values of the critical point. Thus, the special third-grade fluid accelerates the boundary layer separation.

Table 2: Values of skin friction, Nusselt number and Sherwood number for different values of K when $Nb = 1, Nt = 1.5, Le = 1, Q_w = 1.5, R_d = 2, \gamma = 0.3$ are fixed.

S	K	$C_f \mathrm{Re}_x^{1/2}$		$Nu_x Re_x^{-1/2}$		$Sh_x \mathrm{Re}_x^{-1/2}$	
		First solution	Second solution	First solution	Second solution	First solution	Second solution
2.8	0	2.3798	0.1577	1.0749	1.0454	2.2400	1.8205
	1	1.3511	0.1658	1.0725	1.0456	2.1844	1.8223
	2	1.1227	0.1746	1.0712	1.0459	2.1593	1.8244
2.6	0	2.1307	0.3247	1.0669	1.0293	2.0228	1.6267
	1	1.2573	0.3209	1.0634	1.0296	1.9643	1.6279
	2	1.0446	0.3198	1.0615	1.0299	1.9355	1.6297
2.4	0	1.8633	0.4670	1.0554	1.0094	1.7984	1.4472
	1	1.1439	0.4479	1.0501	1.0101	1.7349	1.4493
	2	0.9466	0.4386	1.0469	1.0111	1.7000	1.4530
2.2	0	1.5583	0.6140	1.0374	0.9886	1.5592	1.2916
	1	0.9858	5868	1.0277	0.9921	1.4829	1.3018
	2	0.7860	0.5914	1.0192	0.9977	1.4269	1.3217

Table 3: Critical values of S_c for different values of K when $Nb = 1, Nt = 1.5, Le = 1, Q_w = 1.5, R_d = 2, \gamma = 0.3$ are fixed.

K	S_c
0	1.9990
1	2.0950
2	2.1636

5 Conclusions

This research analyzed the boundary layer flow with heat and mass transfer of a special third-grade fluid over a heated shrinking sheet with nonlinear thermal radiation. The transformed ordinary differential equations are numerically solved using shooting method for different values of the pertinent parameters. From this study, the following conclusions can be drawn:

1. Dual solutions are achieved for certain values of the suction parameter.
2. Due to the non-Newtonian parameter, the velocity of the fluid decreases for the first solution and decreases for the second solution. On the other hand, the temperature and concentration profiles increase for the first solution and decrease for the second solution.
3. The thermal and concentration boundary layer thicknesses are enhanced due to the convective parameter for the first and the second solutions.
4. The thermal radiation reduces the temperature of the fluid as well as the nanoparticles concentration for both solutions.
5. Using the Brownian motion mechanism, the distribution of nanoparticles can be arranged in the flow regime by taking larger values of Nb or Nt and also cooling of the regime can be achieved by taking smaller values of Nb or Nt.

We believe that the present results may be used for explaining the non-Newtonian characteristics and applications in the tribology field, automotive industry, etc. For example, in machineries, the lubricating oils are tested frequently for viscosity as it may affect the oil performance and thus influence the equipment life span. Since oils are utilized for a long period of time and still being used, factors involving the particles of contamination and smoke from unfinished combustion, may reason them to acquire on more characteristics of a non-Newtonian fluid at the lower shear rates. Therefore, the involved physical parameters and suitable situations for instance, shrinking sheets, adequate suction, etc. require to be handled and applied in order to organize the non-Newtonian behavior of the oil.

References

[1] Ellahi R, Hayat T, Mahomed FM. Generalized Couette flow of a third-grade fluid with slip: The exact solutions. Z Naturforsch 2010, 65a, 1071–1076.
[2] Abbasbandy S, Hayat T. On series solution for unsteady boundary layer equations in a special third grade fluid. Comm Nonlinear Sci Numer Simulat 2011, 16, 3140–3146.
[3] Kecebas A, Yurusoy M. Similarity solutions of unsteady boundary layer equations of a special third grade fluid. Int J Eng Sci 2006, 44, 721–729.
[4] Ariel PD. Flow of a third grade fluid through a porous flat channel. Int J Eng Sci 2003, 41, 1267–1285.

[5] Hayat T, Ellahi R, Ariel PD, Asghar S. Homotopy solution for the channel flow of a third grade fluid. Nonlinear Dynam 2006, 45, 55–64.
[6] Naganthran K, Nazar R, Pop I. Unsteady stagnation-point flow and heat transfer of a special third grade fluid past a permeable stretching/shrinking sheet. Scientific Reports 2016, 6, 1–13.
[7] Masuda H, Teramae AEK, Hishinuma N. Alteration of thermal conductivity and viscosity of liquid by dispersing ultra-fine particles. Netsu Bussei 1993, 7, 227–233.
[8] Buongiorno J. Convective transport in nanofluids. ASME J Heat Transf 2006, 128, 240–250.
[9] Khan WA, Pop I. Boundary-layer flow of a nanofluid past a stretching sheet. Int J Heat Mass Transf 2010, 53, 2477–**2483.**
[10] Rana P, Bhargava R. Flow and heat transfer of a nanofluid over a nonlinearly stretching sheet: A numerical study. Commun Nonlin Sci Num Simul 2012, 17, 212–226.
[11] Makinde OD, Aziz A. Boundary layer flow of a nanofluid past a stretching sheet with a convective boundary condition. Int J Thermal Sci 2011, 50, 1326–1332.
[12] Chamkha AJ, Rashad AM, Al-Meshaiei E. Melting effect on unsteady hydromagnetic flow of a nanofluid past a stretching sheet. Int J Chem React Eng 2011, 9, 1–23.
[13] Chamkha AJ, Abbasbandy S, Rashad AM, Vajravelu K. Radiation effects on mix convection over a wedge embedded in a porous medium filled with a nanofluid. Transp Porous Med 2012, 91, 261–279.
[14] Chamkha AJ, Rashad AM, Ram Reddy Ch, Murthy PVSN. Effect of suction/ injection on free convection along a vertical plate in a nanofluid saturated non-Darcy porous medium with internal heat generation. Indian J Pure Appl Math 2014, 45, 321–342.
[15] Gireesha BJ, Chamkha AJ, Rudraswamy NG, Krishnamurthy MR, MHD flow and heat transfer of a nanofluidembedded with dust particles over a stretching sheet. J Nanofluids 2015, 4, 66–72.
[16] Krishnamurthy MR, Gireesha BJ, Prasannakumara BC, Gorla RSR. Thermal radiation and chemical reaction effects on boundary layer slip flow and melting heat transfer of nanofluid induced by a nonlinear stretching sheet. Nonlinear Eng 2016, 5, 147–159.
[17] Aziz A. A similarity solution for laminar thermal boundary layer over a flat plate with a convective surface boundary condition. Commun Nonlinear Sci Numer Simul 2009, 14, 1064–1068.
[18] Makinde OD, Aziz A. MHD mixed convection from a vertical plate embedded in a porous medium with a convective boundary condition. Int J Thermal Sci 2010, 49, 1813–1820.
[19] Ishak A. Similarity solutions for flow and heat transfer over a permeable surface with convective boundary condition. Appl Math Comput 2014, 217, 837–842.
[20] Yao S, Fang T, Zhong Y. Heat transfer of a generalized stretching/shrinking wall problem with convective boundary conditions. Commun Nonlinear Sci Numer Simul 2011, 16, 752–760.
[21] Rahman MM, Merkin JH, Pop I. Mixed convection boundary-layer flow past a vertical flat plate with a convective boundary condition. Acta Mech 2015, 226, 2441–2460.
[22] Mustafa M, Khan JA, Hayat T, Alsaedi A. Simulations for Maxwell fluid flow past a convectively heated exponentially stretching sheet with nanoparticles. AIP Advances 2015, 5, 037133.
[23] W. Ibrahim, R.U. Haq, Magnetohydrodynamic (MHD) stagnation point flow of nanofluid
past a stretching sheet with convective boundary condition. J Braz Soc Mech Sci Eng 2016, 38, 1155–1164.
[24] Makinde OD, Khan WA, Khan ZH. Stagnation point flow of MHD chemically reacting nanofluid over a stretching convective surface with slip and radiative heat. Proc IMechE Part E: J Process Mech Eng 2016, 0, 1–9.
[25] Khan M, Hashim, Hussain M, Azam M, Magnetohydrodynamic flow of Carreau fluid over a convectively heated surface in the presence of non-linear radiation. J Magn Magn Mater 2016, 412, 63–68.
[26] Makinde OD, Aziz A. Boundary layer flow of a nanofluid past a stretching sheet with a convective boundary condition. Int J Thermal Sci 2011, 50, 1326–1332.
[27] Merkin JH. On dual solutions occurring in mixed convection in a porous medium. J Eng Math 1986, 20(2), 171–179.
[28] Weidman PD, Kubitschek DG, Davis AMJ. The effect of transpiration on self-similar boundary layer flow over moving surfaces. Int J Eng Sci 2006, 44(11-12), 730–737.
[29] Harris SD, Ingham DB, Pop I. Mixed convection boundary-layer flow near the stagnation point on a vertical surface in a porous medium: Brinkman model with slip. Transp Porous Med 2009, 77(2), 267–285.